arXiv:2008.05780v1 [eess.IV] 13 Aug 2020

Multi-Modality Pathology Segmentation Framework: Application to Cardiac Magnetic Resonance Images

Zhen Zhang[1], Chenyu Liu[1], Wangbin Ding[1], Sihan Wang[2], Chenhao Pei[1], Mingjing Yang[1,*], and Liqin Huang[1]

[1] College of Physics and Information Engineering, Fuzhou University, Fuzhou, China
[2] School of Basic Medical Science, Fudan University, Shanghai, China

Abstract. Multi-sequence of cardiac magnetic resonance (CMR) images can provide complementary information for myocardial pathology (scar and edema). However, it is still challenging to fuse these underlying information for pathology segmentation effectively. This work presents an automatic cascade pathology segmentation framework based on multi-modality CMR images. It mainly consists of two neural networks: an anatomical structure segmentation network (ASSN) and a pathological region segmentation network (PRSN). Specifically, the ASSN aims to segment the anatomical structure where the pathology may exist, and it can provide a spatial prior for the pathological region segmentation. In addition, we integrate a denoising auto-encoder (DAE) into the ASSN to generate segmentation results with plausible shapes. The PRSN is designed to segment pathological region based on the result of ASSN, in which a fusion block based on channel attention is proposed to better aggregate multi-modality information from multi-modality CMR images. Experiments from the MyoPS2020 challenge dataset show that our framework can achieve promising performance for myocardial scar and edema segmentation.

Keywords: Myocardial pathology · Multi-sequence CMR · Segmentation.

1 Introduction

Myocardial infarction (MI) is one of the most dangerous cardiovascular diseases in worldwide. The severity of MI depends on the assessment of the myocardial scar and edema [3]. Accurate delineation of these pathological regions from cardiac magnetic resonance (CMR) can provide important advancements for the prediction and management of MI patients [5]. Since manual delineation is generally time-consuming, tedious and subject to inter-observer variations, the automatic segmentation approach has gradually attracted more attention of research.

* M Yang is the corresponding authors: yangmj5@fzu.edu.cn

Conventional myocardial pathology segmentation methods are mainly based on intensity thresholding, such as the signal threshold to reference mean (STRM) [6], region growing (RG) [1] and full-width at half-maximum (FWHM) [2]. However, the thresholding methods could be easily affected by the image noise, and have poor agreement with expert delineations [9,16]. Recently, learning-based methods have achieved promising performance in different pathology segmentation tasks, such as brain tumor [10] and liver lesion [15]. For pathology segmentation on left atrium (LA) myocardium, Yang et al. presented a super-pixel scar segmentation method using support vector machine (SVM) [11]. Li et al. proposed a fully automated scar segmentation method based on the graph-cuts framework, where the potentials of the graph are estimated via deep neural network (DNN) [8]. Futhermore, Li et al. designed a multi-task learning network to joint perform LA segmentation and LA scars quantification, in which the LA boundary is extracted as spatial attention for the scars [7]. For pathology segmentation on left ventricular (LV) myocardium, Zabihollahy et al. proposed a CNN-based method to segment scar from late gadolinium enhancement (LGE) MRIs [14]. However, their method relies on the manual delineation of the LV myocardium region. To achieve a fully automatic scar segmentation method, they further developed a multi-planar network to segment LV myocardium [13].

At present, most DNN-based myocardial pathology segmentation methods are focus on mono-modality CMR, such as LGE. But multi-modality CMR can provide different enhanced-information of the whole heart. For instance, the balanced-Steady State Free Precession (bSSFP) cine sequence can present a clear myocardial boundary, while the LGE and T2-weighted CMR can highlight the scar and edema regions, respectively [19,20]. Being aware that the complementary information is helpful for myocardial pathology segmentation. We design a cascade multi-modality pathology segmentation framework. Figure 1 shows the overview of the framework. The framework decomposes the pathology segmentation task into two sub-stages, i.e. the anatomical structure segmentation stage and the pathological region segmentation stage. The main contributions of our work are:

(1) we propose a fully automatic pathology segmentation framework, and validate it using the MyoPS2020 challenge dataset [1].

(2) we present an anatomical structure segmentation network, where a denoising auto-encoder (DAE) is adopted to reconstruct the segmentation results with realistic shapes.

(3) we propose a pathological region segmentation network, in which a channel attention based fusion block is designed to adaptively fuse complementary information of multi-modality CMR images for pathology segmentation.

[1] http://www.sdspeople.fudan.edu.cn/zhuangxiahai/0/MyoPS20/

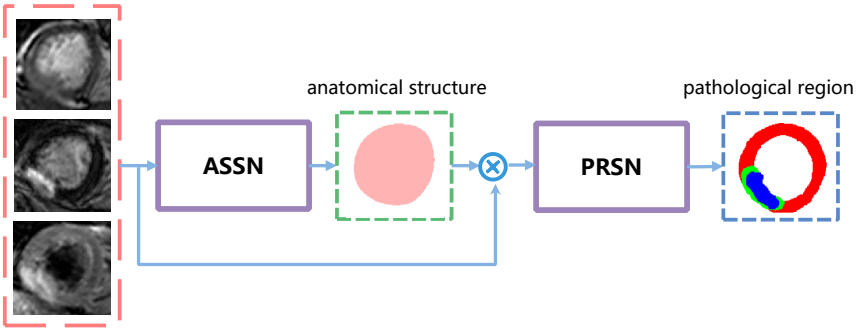


Fig. 1. The architecture of the multi-modality pathology segmentation framework. Given multi-modality CMR (bSSFP, T2, DE) images, the ASSN first obtains a candidate anatomical structure, where the pathology may exist. Then, the PRSN predicts the final scar and edema regions within the candidate structure.

2 Method

2.1 Anatomical Structure Segmentation Network (ASSN)

The ASSN is designed to obtain a candidate anatomical structure from CMR images. In the myocardial pathology segmentation task, we designate the candidate structure as the LV epicardial region, where the scar and edema may exist. Figure 2 shows the architecture of the ASSN. It mainly includes three individual encoders and one shared decoder. Each encoder can obtain underlying anatomical feature from CMR, while the decoder can fuse the obtained features, and predicts a pixel-level LV mask.

Given a multi-modality CMR images I=(I_{bSSFP}, I_{LGE}, I_{T2}), the ASSN aims to learn a mapping f_θ from I to a binary mask. Therefore, the network can be trained under supervised manner, and the loss function is

$$\mathcal{L}oss_{seg} = \mathcal{D}ice(f_\theta(I), L_{lv}) \tag{1}$$

where the L_{lv} is the golden standard of the LV, $\mathcal{D}ice(A, B)$ refers to the Dice score of A and B. Thus, the candidate anatomical structure C=(C_{bSSPF}, C_{LGE}, C_{T2}) can be extracted as

$$C_{bSSFP} = I_{bSSFP} \otimes f_\theta(I), \tag{2}$$

$$C_{LGE} = I_{LEG} \otimes f_\theta(I), \tag{3}$$

$$C_{T2} = I_{T2} \otimes f_\theta(I), \tag{4}$$

where $\otimes$ is element-wise multiplication.

Generally, the ASSN performs pixel-wise classification based on processing the intensity value of I. However, the pathology usually leads to abnormal intensity distribution in CMR images. For instance, LGE visualizes the scars as brighter texture, in contrast to the dark healthy myocardium [21]. Therefore, the

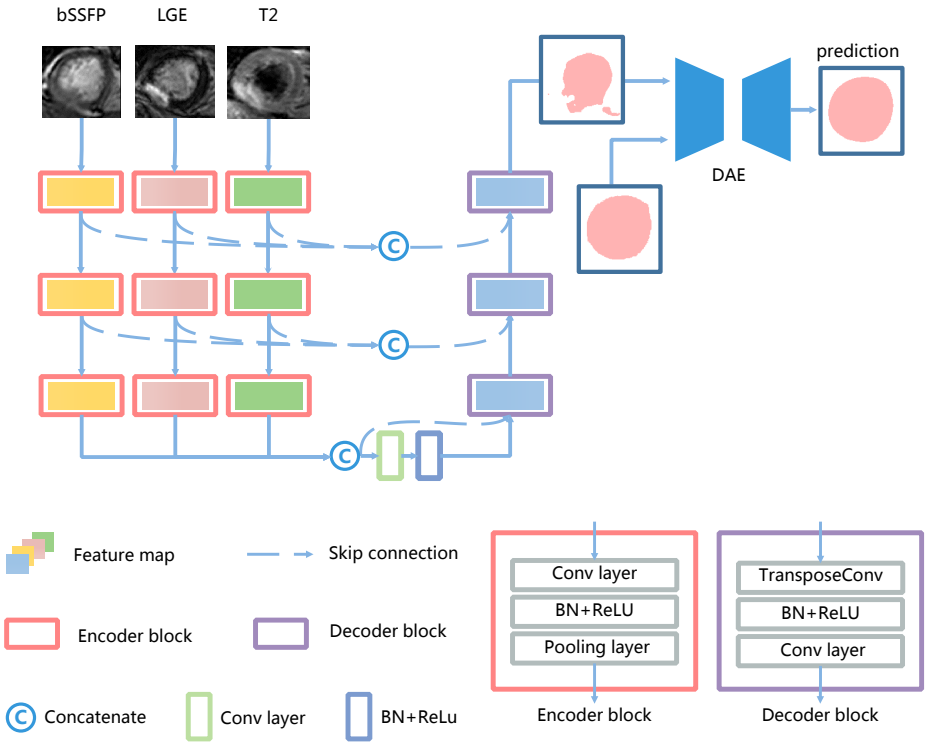


Fig. 2. The architecture of the ASSN. The auxiliary DAE is adopted to suppress the influence of the pathology region and generate results with plausible shape.

segmentation results could be easily affected. To tackle this, we adopt a DAE to refine the segmentation results with realistic shapes [12].

A DAE usually follows an encoder-decoder (E-D) architecture. Let the $\ddot{L}$ denotes the noisy version of the L_{gd}, the DAE aims to map the $\ddot{L}$ to a lower-dimension representation h, from which the L_{gd} can be reconstructed. It can be trained to minimize the reconstruction error of the input

$$\mathcal{L}oss_{DAE} = \|D(E(\ddot{L})) - L_{gd}\|_2, \tag{5}$$

where $E(\ddot{L})$ is a compact representation of $\ddot{L}$, $D(E(\ddot{L}))$ is a reconstruction of L_{gd}. Regarding the original segmentation result $f_\theta(I)$ as a noisy version of the golden standard label, we integrate the DAE into the ASSN to reconstruct the original result into a plausible one. So that, the final loss function of the ASSN is defined as

$$\mathcal{L}oss_{ASSN} = \mathcal{L}oss_{seg} + \beta\mathcal{D}ice(D(E(f_\theta(I))), L_{lv}), \tag{6}$$

where β is the balance coefficient between the Dice loss and reconstruction loss.

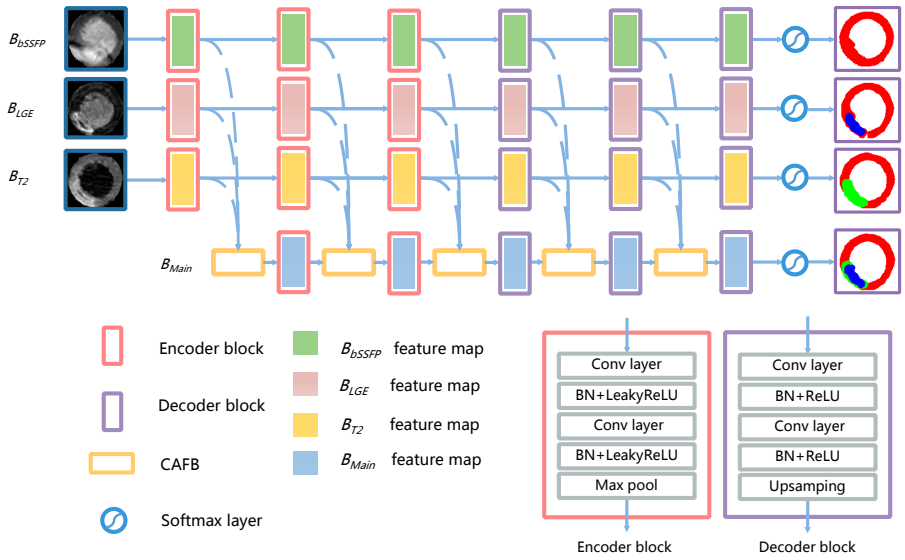


Fig. 3. The architecture of PRSN. It contains four sub-branches B_{bSSFP}, B_{LEG}, B_{T2}, B_{Main}. We set up to segment the myocardium in B_{bSSFP}; the scars and normal myocardium in B_{LEG}; the edema and normal myocardium in B_{T2}; the scars, edema and normal myocardium in B_{Main}.

2.2 Pathological Region Segmentation Network (PRSN)

In the pathological region segmentation network (PRSN), complementary information from $C = (C_{bSSPF}, C_{LGE}, C_{T2})$ are expected to be fused and boost the pathology segmentation performance. Figure 3 shows the architecture of PRSN. We construct three DNN branches $(B_{bSSPF}, B_{LGE}, B_{T2})$ to capture multi-modality information from each candidate region. Specifically, the B_{LEG} and B_{T2} mainly aim to acquire pathology (scar and edema) features from C_{LGE} and C_{T2}. Meanwhile, the B_{bSSFP} is intent to obtain myocardium features from C_{bSSPF}. Due to most of the scar and edema are scatted in the myocardium, the myocardium features can provide spatial prior information for the pathology regions. Therefore, the cost functions of three DNN branches are

$$\mathcal{L}oss_{bSSFP} = \mathcal{D}ice(L_{bSSFP}, \hat{L}_{bSSFP}), \tag{7}$$

$$\mathcal{L}oss_{LGE} = \mathcal{D}ice(L_{LGE}, \hat{L}_{LGE}), \tag{8}$$

$$\mathcal{L}oss_{T2} = \mathcal{D}ice(L_{T2}, \hat{L}_{T2}), \tag{9}$$

where L_{bSSFP} (L_{LGE}, L_{T2}) and $\hat{L}_{bSSFP}$ ($\hat{L}_{LGE}$, $\hat{L}_{T2}$) are corresponding gold standard and predicted label of B_{bSSPF} (B_{LEG}, B_{T2}) branch, respectively.

Having the three sub-branches constructed, the potential features from them are need be fused and propagated to a main-branch B_{Main} for pathology segmenting. At present, the most popular feature fusion strategies include summation, product and maximization. However, they still suffer from the lack of

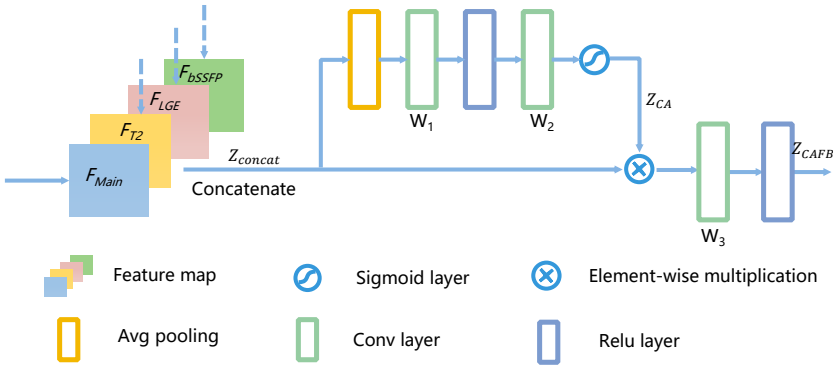


Fig. 4. The channel-wise fusion block

robustness in different tasks [17]. As shown in the Figure 4, we propose a multi-modality channel-attention fusion block (CAFB) for adaptively weighted feature fusion of different modalities in B_{Main}.

Suppose we have three feature maps ($F_{bSSFP}, F_{LGE}, F_{T2}$) from sub-branches and one previous output F_{Main} of the main-branch, the CAFB first merges these feature maps to obtain an concatenated feature Z_{concat}. Since Z_{concat} aggregates all feature maps from (B_{bSSFP}, B_{LEG}, B_{T2}), it easily suffers from the information redundancy. Due to the channel-attention (CA)[4] can emphasize informative features and suppress less useful ones, the block adopts it to performs channel-wise feature re-calibration on $Z_{concate}$. So That, the output of CAFB (Z_{CAFB}) is

$$Z_{CA} = \delta(W_2\sigma(W_1 Avg(Z_{concat})), \tag{10}$$

$$Z_{CAFB} = \sigma(W_3(Z_{CA} \otimes Z_{concat})), \tag{11}$$

where σ, δ and Avg refer to Relu, Sigmoid and average pooling function, respectively; and W_1, W_2 and W_3 are parameters of different convolution layers. Here, Z_{CA} is the channel-wise attention weight, with which the original Z_{concat} can be re-calibrated and achieve better representation of multi-modality information.

Furthermore, we apply the CAFB in different hierarchies of the B_{Main} (see B_{Main} in Figure 3). Thus, the B_{Main} can capture multi-scale multi-modality features for pathology segmentation. The training loss of the B_{Main} can be defined as

$$\mathcal{L}oss_{Main} = \mathcal{D}ice(L_{Main}, \hat{L}_{Main}), \tag{12}$$

where L_{Main} and $\hat{L}_{Main}$ are the gold standard and predicted label of B_{Main}, respectively. Note that the B_{Main} jointly performs scar, edema and normal myocardium segmentation. Finally, the overall loss function of the PRSN is

$$\mathcal{L}oss_{PRSN} = \mathcal{L}oss_{Main} + \lambda_{bSSFP}\mathcal{L}oss_{bSSFP} + \lambda_{LGE}\mathcal{L}oss_{LEG} + \lambda_{T2}\mathcal{L}oss_{T2}, \tag{13}$$

where λ_{bSSFP}, λ_{LGE} and λ_{T2} are hyper-parameters.

3 Experiment

3.1 Dataset

The framework was evaluated in the MyoPS2020 challenge data set which contains 45 multi-sequence CMR (bSSFP, LGE, T2) images. In our experiments, the training and validation sets comprise 20 and 5 images with their gold standard labels, respectively. The testing set includes 20 images. All published data has been aligned in a common space and resampled with the same spatial resolution. For evaluation, we randomly selected 20 samples for training networks, while leaving the rest of 5 samples for validation.

3.2 Implementations

We trained our models by extracting 2D slices from multi-sequence CMR images. Each slice was cropped and resized to 128×128 pixels which are roughly centering at the heart region. All of the models (DAE, ASSN and PRSN) were implemented in Python and optimized by using the Adam algorithm.

For the DAE: In each training iteration, we generated $\ddot{L}$ by randomly adding noise to a gold standard label L. Having a pair of (L, $\ddot{L}$) prepared, the DAE can be trained via minimizing the reconstruction loss $\mathcal{L}oss_{DAE}$ (see Eq.5).

For the ASSN: The pre-trained DAE was adopted to perform shape reconstruction. In each training iteration, the sample $I = (I_{bSSFP}, I_{LGE}, I_{T2}, L)$ was feed into the network. By setting the β to 0.2 in $\mathcal{L}_{ASSN}$ (see Eq.6), the trainable loss can be calculated and back-propagated to optimize the parameters of ASSN.

For the PRSN: We first extracted $C = (C_{bSSPF}, C_{LGE}, C_{T2})$ and their corresponding label $(L_{bSSPF}, L_{LGE}, L_{T2})$ from the training data. Then, the hyper-parameter λ_{bSSFP}, λ_{LGE} and λ_{T2} were set to 0.3, 0.5 and 0.5, respectively (see Eq. 13). Finally, the network can be trained by minimizing the $\mathcal{L}oss_{PRSN}$.

3.3 Results

ASSN: To evaluate the performance of the ASSN, the Dice score and Hausdorff distance between the predicted label and gold standard label were calculated. Table 1 shows the performance of three different methods:

- Unet-bSSFP: The Unet which is trained by using bSSFP images. We implemented this method because the bSSFP can provide a relatively clear boundary of the LV.
- ASSN-WO-DAE: Our ASSN network but without DAE.
- ASSN: Our proposed anatomical structure segmentation network.

Compared to Unet-bSSFP, the methods (ASSN-WO-DAE and ASSN) using multi-modality CMRs can achieve better performance in both terms of Dice score and Hausdorff distance. Additionally, although the ASSN-WO-DAE obtained comparable result to ASSN in term of the Dice score, the ASSN still

Table 1. Dice score and Hausdorff of the proposed method and other baseline methods on the validation set.

Method	Dice (%)	Hausdorff (mm)
Unet-bSSFP	93.77 ± 2.55	10.72 ± 9.02
ASSN-WO-DAE	96.21 ± 3.28	8.25 ± 9.06
ASSN	**96.99 ± 1.49**	**3.04 ± 0.76**

achieved almost 5 mm improvement in the Hausdorff distance. Moreover, Figure 5 presents a series of visual results. One can see the results of Unet-bSSFP and ASSN-WO-DAE were easily affected by the quality of CMRs, while our ASSN can generate results with plausible shape. This demonstrates the benefit of integrating DAE to the segmentation network.

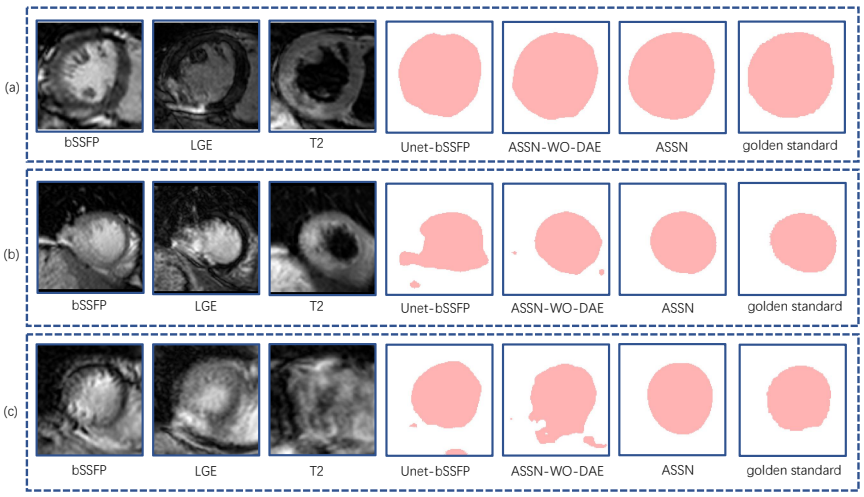


Fig. 5. Comparison of the proposed method and other baseline methods. Image of (a) is a normal case, where all three methods can achieve a reasonable segmentation result. However, the image of (b) and (c) are challenging cases, where both Unet-bSSFP and ASSN -WO-DAE failed to generate realistic results but the proposed ASSN method showed good robustness.

PRSN: The performance of the PRSN is evaluated by the Dice score of scar and scar + edema region. Table 2 shows seven different segmentation methods based on our extracted LV.

- Unet-scar: Unet which is trained on C_{LGE} datas for scar segmentation.
- Unet-edema: Unet which is trained on C_{T2} datas for edema segmentation.
- PRSN-B_{T2}: The B_{T2} branch of PRSN.

Table 2. Dice scores of the proposed method and other baseline methods on the testing set. N/A indicates the segmentation result was not provided

Method	scar (%)	edema (%)
Unet-edema	N/A	61.42 ± 11.86
Unet-scar	56.38 ± 23.36	N/A
PRSN-B_{T2}	N/A	64.37 ± 11.25
PRSN-B_{LGE}	55.65 ± 24.97	N/A
	scar (%)	scar + edema (%)
Fusion-Unet	57.50 ± 23.09	66.61 ± 12.79
MFB-PRSN	59.56 ± 25.18	68.59 ± 12.33
PRSN	**64.09 ± 25.96**	**70.24 ± 12.98**

- PRSN-B_{LGE}: The B_{LGE} branch of PRSN.
- Fusion-Unet: Unet which is implemented by using input-level fusion strategy [18].
- MFB-PRSN: PRSN which is implemented by using MFB (summation-product-maximization) fusion strategy in B_{Main} [17].
- PRSN: Our proposed pathological region segmentation network.

Among these methods, the Unet-scar, Unet-edema, PRSN-B_{T2} and PRSN-B_{LGE} can be considered as the mono-modality methods, while the MFB-PRSN, Fusion-Unet and PRSN are multi-modality methods. Overall, the multi-modality methods achieved better results than the mono-modality methods in scar segmentation. This reveals the advantage of using multi-modality images for pathology segmentation. Meanwhile, compared to MFB-PRSN which uses the summation-product-maximization fusion strategy for feature fusion, our PRSN achieved almost 4% and 3% improvement in scar and scar + edema region, respectively. This indicates the advantage of our proposed CAFB. In addition, Figure 6 demonstrates visual results of different methods.

4 Conclusion

In this work, we proposed a cascade multi-modality pathology segmentation framework. It has been evaluated on scar and edema segmentation of CMR images. The experimental results show our CAFB is capable in fusing complementary information from multi-sequence CMRs to boost the pathology segmentation performance. Besides, we present the advantage of using DAE to reconstruct the segmentation result with plausible shape. Future research aims to investigate the performance of the framework on other pathological datasets.

References

1. Albà, X., i Ventura, R.M.F., Lekadir, K., Frangi, A.F.: Healthy and scar myocardial tissue classification in de-mri. In: International Workshop on Statistical Atlases and Computational Models of the Heart. pp. 62–70. Springer (2012)

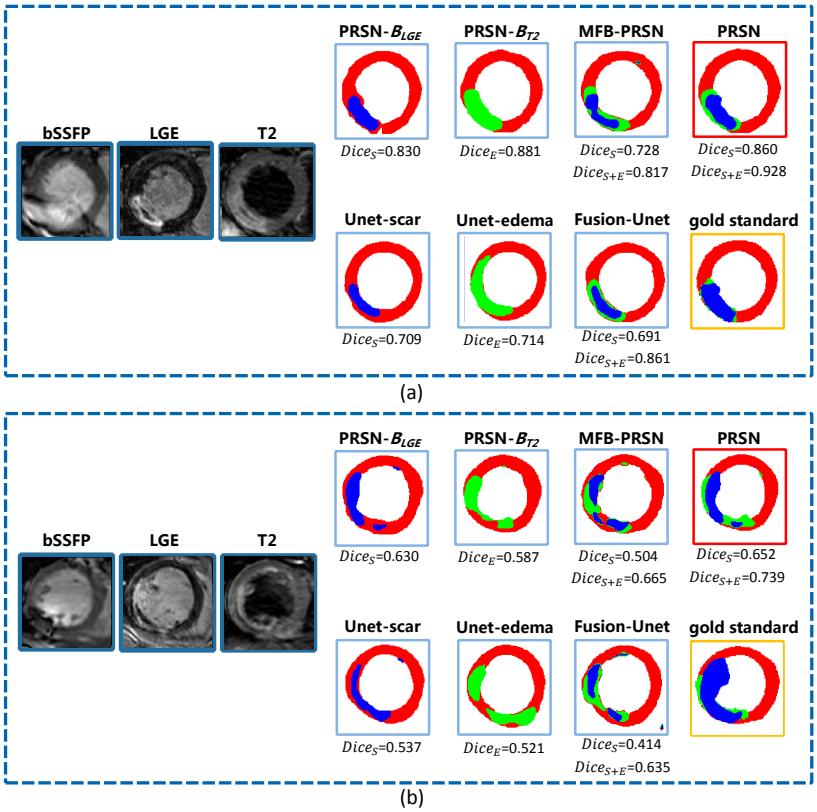


Fig. 6. Visualization of the pathology segmentation results. The $Dice_S$, $Dice_E$ and $Dice_{S+E}$ refer to the Dice score of predicted scar (blue), edema (green) and scar + edema region, respectively. Image of (a) is an easy case, while the image of (b) is a more challenging one. (The reader is referred to the colourful web version of this article.)

2. Amado, L.C., Gerber, B.L., Gupta, S.N., Rettmann, D.W., Szarf, G., Schock, R., Nasir, K., Kraitchman, D.L., Lima, J.A.: Accurate and objective infarct sizing by contrast-enhanced magnetic resonance imaging in a canine myocardial infarction model. Journal of the American College of Cardiology **44**(12), 2383–2389 (2004)
3. Berry, C., Kellman, P., Mancini, C., Chen, M.Y., Bandettini, W.P., Lowrey, T., Hsu, L.Y., Aletras, A.H., Arai, A.E.: Magnetic resonance imaging delineates the ischemic area at risk and myocardial salvage in patients with acute myocardial infarction. Circulation: Cardiovascular Imaging **3**(5), 527–535 (2010)
4. Hu, J., Shen, L., Sun, G.: Squeeze-and-excitation networks. In: Proceedings of the IEEE conference on computer vision and pattern recognition. pp. 7132–7141 (2018)
5. Ingkanisorn, W.P., Rhoads, K.L., Aletras, A.H., Kellman, P., Arai, A.E.: Gadolinium delayed enhancement cardiovascular magnetic resonance correlates with clinical measures of myocardial infarction. Journal of the American College of Cardiology **43**(12), 2253–2259 (2004)

6. Kolipaka, A., Chatzimavroudis, G.P., White, R.D., ODonnell, T.P., Setser, R.M.: Segmentation of non-viable myocardium in delayed enhancement magnetic resonance images. The international journal of cardiovascular imaging **21**(2-3), 303–311 (2005)
7. Li, L., Weng, X., Schnabel, J.A., Zhuang, X.: Joint left atrial segmentation and scar quantification based on a dnn with spatial encoding and shape attention. arXiv preprint arXiv:2006.13011 (2020)
8. Li, L., Wu, F., Yang, G., Xu, L., Wong, T., Mohiaddin, R., Firmin, D., Keegan, J., Zhuang, X.: Atrial scar quantification via multi-scale cnn in the graph-cuts framework. Medical image analysis **60**, 101595 (2020)
9. Spiewak, M., Malek, L.A., Misko, J., Chojnowska, L., Milosz, B., Klopotowski, M., Petryka, J., Dabrowski, M., Kepka, C., Ruzyllo, W.: Comparison of different quantification methods of late gadolinium enhancement in patients with hypertrophic cardiomyopathy. European journal of radiology **74**(3), e149–e153 (2010)
10. Wang, G., Li, W., Ourselin, S., Vercauteren, T.: Automatic brain tumor segmentation using cascaded anisotropic convolutional neural networks. In: International MICCAI brainlesion workshop. pp. 178–190. Springer (2017)
11. Yang, G., Zhuang, X., Khan, H., Haldar, S., Nyktari, E., Li, L., Wage, R., Ye, X., Slabaugh, G., Mohiaddin, R., et al.: Fully automatic segmentation and objective assessment of atrial scars for long-standing persistent atrial fibrillation patients using late gadolinium-enhanced mri. Medical physics **45**(4), 1562–1576 (2018)
12. Yue, Q., Luo, X., Ye, Q., Xu, L., Zhuang, X.: Cardiac segmentation from lge mri using deep neural network incorporating shape and spatial priors. In: International Conference on Medical Image Computing and Computer-Assisted Intervention. pp. 559–567. Springer (2019)
13. Zabihollahy, F., Rajchl, M., White, J.A., Ukwatta, E.: Fully automated segmentation of left ventricular scar from 3d late gadolinium enhancement magnetic resonance imaging using a cascaded multi-planar u-net (cmpu-net). Medical Physics **47**(4), 1645–1655 (2020)
14. Zabihollahy, F., White, J.A., Ukwatta, E.: Convolutional neural network-based approach for segmentation of left ventricle myocardial scar from 3d late gadolinium enhancement mr images. Medical physics **46**(4), 1740–1751 (2019)
15. Zeng, Q., Karimi, D., Pang, E.H., Mohammed, S., Schneider, C., Honarvar, M., Salcudean, S.E.: Liver segmentation in magnetic resonance imaging via mean shape fitting with fully convolutional neural networks. In: International Conference on Medical Image Computing and Computer-Assisted Intervention. pp. 246–254. Springer (2019)
16. Zhang, L., Huttin, O., MARIE, P.Y., Felblinger, J., Beaumont, M., CHILLOU, C.D., Girerd, N., Mandry, D.: Myocardial infarct sizing by late gadolinium-enhanced mri: Comparison of manual, full-width at half-maximum, and n-standard deviation methods. Journal of Magnetic Resonance Imaging **44**(5), 1206–1217 (2016)
17. Zhou, T., Fu, H., Chen, G., Shen, J., Shao, L.: Hi-net: hybrid-fusion network for multi-modal mr image synthesis. IEEE transactions on medical imaging (2020)
18. Zhou, T., Ruan, S., Canu, S.: A review: Deep learning for medical image segmentation using multi-modality fusion. Array **3**, 100004 (2019)
19. Zhuang, X.: Multivariate mixture model for cardiac segmentation from multi-sequence mri. In: International Conference on Medical Image Computing and Computer-Assisted Intervention. pp. 581–588. Springer (2016)

20. Zhuang, X.: Multivariate mixture model for myocardial segmentation combining multi-source images. IEEE transactions on pattern analysis and machine intelligence **41**(12), 2933–2946 (2019)
21. Zhuang, X., Xu, J., Luo, X., Chen, C., Ouyang, C., Rueckert, D., Campello, V.M., Lekadir, K., Vesal, S., RaviKumar, N., et al.: Cardiac segmentation on late gadolinium enhancement mri: A benchmark study from multi-sequence cardiac mr segmentation challenge. arXiv preprint arXiv:2006.12434 (2020)